AIChE WILEY InterScience DISCOVER SOMETHING GREAT

FLUID MECHANICS AND TRANSPORT PHENOMENA

Polymer Flocculation of Calcite: Population Balance Model

Alex R. Heath
A. J. Parker Cooperative Research Centre for Hydrometallurgy (CSIRO Minerals), Clayton South, Victoria, Australia

Parisa A. Bahri
A. J. Parker Cooperative Research Centre for Hydrometallurgy (Murdoch University), School of Engineering-Rockingham Campus, Western Australia

Phillip D. Fawell and John B. Farrow
A. J. Parker Cooperative Research Centre for Hydrometallurgy (CSIRO Minerals), Waterford, Western Australia

DOI 10.1002/aic.10749
Published online January 10, 2006 in Wiley InterScience (www.interscience.wiley.com).

A population balance (PB) model is used to describe the aggregation/breakage kinetics of calcite flocculation in turbulent pipe flow. The model describes simultaneous aggregation and breakage, and accounts for likely process variables: fluid shear, flocculant dosage, primary particle size and solid fraction, using four fitted parameters. Particle collision is described by the turbulent collision kernel of Saffman and Turner,[1] however, the capture efficiency (α) is initially set to equal zero until the point of flocculant addition, then increases rapidly as described by an equation accounting for flocculant mixing/adsorption. Particles aggregated by high-molecular weight polymer flocculant typically do not achieve a steady-state aggregate size, where the rates of aggregation and breakage are equal. Instead, the aggregate size decreases gradually due to polymer chain scission or rearrangement on repeated aggregation/breakage. This phenomenon is accounted for in the model by a flocculant strength degradation term. © 2006 American Institute of Chemical Engineers *AIChE J,* 52: 1641-1653, 2006
Keywords: flocculation, population balance modeling, reaction kinetics, multi-phase flow

Introduction

A population balance is a mathematical model used to describe the change in a particle-size distribution through time. Population balance models have been used to describe a wide range of practical systems, for example: coagulation or flocculation, crystallization, size reduction in grinding mills, and droplet coalescence in solvent extraction or flotation columns.[2,3,4,5] Smoluchowski[6,7] first proposed the population balance approach to flocculation kinetics modeling, and considered three possible mechanisms for particle collision: differential settling, Brownian motion and fluid shear. It is generally accepted[8-12] that fluid shear is the dominant collision mechanism in industrial-scale turbulent flow.

Smoluchowski[6,7] considered the collision rate of particles of differing size in laminar fluid flow, and proposed

$$\beta_{ij} = \frac{4}{3}\gamma(a_i + a_j)^3 \tag{1}$$

where β_{ij} = rate of collision between i and j sized particles (aggregation kernel) ($m^3\ s^{-1}$); γ = laminar shear rate, s^{-1}; a_i = radius of i^{th} particle, m.

Correspondence concerning this article should be addressed to A. R. Heath at alex.heath@csiro.au.

Camp and Stein[13] substituted the term $G = \sqrt{\Phi/\mu}$, the spatially averaged turbulent shear rate

$$\beta_{ij} = \frac{4}{3}\sqrt{\frac{\Phi}{\mu}}(a_i + a_j)^3 \tag{2}$$

where Φ = energy dissipation rate per unit volume, kg m^{-1} s^{-3}; and μ = fluid viscosity, N s m^{-2}.

Camp and Stein's assumptions were too simplistic, and have been critiqued repeatedly.[14-17] However, Camp and Stein's kernel is still widely cited, because it is so similar to the more rigorously derived kernel by Saffman and Turner[1]

$$\beta_{ij} = 1.294\sqrt{\frac{\varepsilon}{\nu}}(a_i + a_j)^3 \tag{3}$$

where ε = local turbulent energy dissipation rate per unit mass, m^2 s^{-3}; and ν = kinematic viscosity, m^2 s^{-1}.

Saffman and Turner's kernel is based on various assumptions[14]; the particles are small relative to the Kolmogoroff microscale, they are neutrally buoyant and spherical, the turbulence is isotropic and homogeneous, the aggregation is slow and there are no hydrodynamic or colloidal interactions between particles. In highly turbulent flows, where the microscale is small, the particles may be larger than the microscale and inertial effects become important. In this case it is generally thought[5,10,11,15,18,19] that the aggregation rate will be proportional to $\varepsilon^{1/3}$.

Despite the various restrictions noted above, Eqs. 2 or 3 have been widely used to describe practical systems[8,11,20-30] although the kernel is usually found to overestimate the actual aggregation rate, and a capture efficiency term (α) is typically used to account for the discrepancy. Colliding particles may be prevented from adhering due to a variety of effects, such as hydrodynamic[17,31,32,33] or electrostatic[34,35] repulsion. Flocculant surface coverage may also play a part and various relationships have been proposed to describe the effect of flocculant surface coverage on the capture efficiency.[36,37,38]

The population balance approach for solving the kernels was first described by Smoluchowski[7] for aggregation only

$$\frac{dN_k}{dt} = \frac{1}{2}\sum_{i=1,i+j=k}^{k-1}\beta_{ij}N_iN_j - \sum_{i=1}^{\infty}\beta_{ik}N_iN_k \tag{4}$$

However, current population balance models for coagulation/flocculation typically also have a capture efficiency term and terms describing aggregate breakage[3,29,30,39,40,41]

$$\frac{dN_k}{dt} = \frac{1}{2}\sum_{i=1,i+j=k}^{k-1}\alpha\beta_{ij}N_iN_j - \sum_{i=1}^{\infty}\alpha\beta_{ik}N_iN_k - S_kN_k + \sum_{l=k+1}^{\infty}\Gamma_{lk}S_lN_l \tag{5}$$

where N_i = number of i^{th} sized particles, m^{-3}; t = time, s; α = capture efficiency [0,1]; β_{ij} = rate of collision between i and j sized particles (aggregation kernel), m^3 s^{-1}; S_k = breakage rate (kernel) of k^{th} sized particles, s^{-1}; Γ_{lk} = breakage distribution function (number of k size particles produced from the breakage of a l sized particle).

Aggregate breakage has received less attention in the literature than aggregation, although there is still a reasonable body of work in the area. Breakage kernel development has aimed to resolve a number of issues: (1) the size and number of daughter fragments, (2) the mechanism of breakage, fluid shear or collisional breakage, (3) the relationship between the shear and breakage rates, and (4) the breakage probability as a function of aggregate size.

A common approach is to assume breakage gives two daughter aggregates of roughly the same size.[3,24,30,42,43] However, more fragments covering a range of sizes have also been used.[23,29,30,40,44-49] Erosion of small fragments, or even primary particles, has also been suggested,[36,50,51,52] although this mechanism is less popular and is not well supported by experimental distributions that generally show smooth bell-shaped distributions without additional peaks at small sizes.

The breakage rate is usually also taken to be a function of the energy dissipation or shear rate. A higher shear rate typically provides rapid initial mixing and faster initial aggregation, but eventually results in smaller aggregates due to increased breakage. This is a typical experimental result,[22,53,54,55] and is usually incorporated into the population balance by assuming

$$S_i \propto \left(\frac{\varepsilon\rho}{\mu}\right)^n \tag{6}$$

where n is a higher exponent than in the aggregation kernel (Eq. 3). That is, an increased shear rate increases both the aggregation and breakage rates, but the breakage term is dominant. Aggregation is usually taken as being directly proportional to $\varepsilon^{0.5}$ (for example, Eq. 3), and n is typically[29,30,56] 0.5–1.

The probability of breakage increases with size and is frequently[29,30,47,56,57] taken to be simply directly proportional to the aggregate diameter. Other more complex relationships have also been proposed, sometimes as a function of the aggregate size in relation to the Kolmogorov microscale.[5,58,59]

Despite the body of work already published in this area, few population balance models simultaneously account for changes to the process variables encountered in practice in mineral processing thickeners/clarifiers (fluid shear rate, flocculant dosage, primary particle size, solid fraction). In addition, most models are written to describe coagulation using soluble salts, where aggregate breakage is reversible. The model presented in this article is specific for flocculation with high-molecular-weight polymer flocculants, as widely used in the mineral processing industry, and accounts for the (partially) irreversible aggregate breakage due to polymer chain scission or rearrangement.

Experimental

Full experimental details of the data presented in this article have been published previously[60] and only a brief summary is given here.

Calcite (calcium carbonate, Commercial Minerals) of various grades and solid concentrations was flocculated with a commercial 30% anionic high-molecular-weight polymer

Table 1. Matrix of Pipe Reactor Experimental Runs

Run No.	Pipe ID (m)	Flow Velocity (m s^{-1})	Solid ϕ (m^3 m^{-3})	Mean d_p (μm)	Floc. Dose (g t^{-1})
1	0.0254	0.461	0.0369	6.59	20.0
2	0.0254	0.461	0.0369	6.59	**40.0**
3	0.0254	0.461	0.0369	6.59	**10.0**
4	0.0254	0.461	0.0369	6.59	**80.0**
5	0.0254	0.461	0.0369	6.59	**5.0**
6	0.0254	0.461	**0.0246**	6.59	20.0
7	0.0254	0.461	**0.0615**	6.59	20.0
8	0.0254	0.461	**0.0123**	6.59	20.0
9	0.0254	0.461	**0.0492**	6.59	20.0
10	0.0254	**0.781**	0.0369	6.59	20.0
11	0.0254	**1.294**	0.0369	6.59	20.0
12	**0.0381**	**0.554**	0.0369	6.59	20.0
13	**0.0381**	**0.343**	0.0369	6.59	20.0
14	**0.0381**	**0.207**	0.0369	6.59	20.0
15	0.0254	0.461	0.0369	**15.08**	20.0
16	0.0254	0.461	0.0369	**2.36**	20.0
17	0.0254	0.461	0.0369	**3.47**	20.0
18	0.0254	0.461	0.0369	**24.26**	20.0
19	0.0254	0.461	**0.0246**	**15.08**	20.0
20	0.0254	**0.781**	0.0369	6.59	**40.0**
21	**0.0381**	**0.343**	0.0369	6.59	**10.0**
22	**0.0381**	**0.343**	**0.0246**	6.59	20.0

(Nalco 9902) in turbulent pipe flow. A range of pipe sizes and flow rates were used to give a range of turbulent shear rates. The pressure drop along the pipe was measured by manometer, allowing the calculation of the shear rate and suspension viscosity. The mean flocculation residence time was varied by changing the length of pipe between the flocculant injection nipple in the side of the pipe, and an online particle-sizing probe (Lasentec® FBRM[61]) placed in-stream at the end of the pipe.

The experimental campaign was according to a sparse matrix of runs (Table 1), with each of the four process variables (fluid shear, flocculant dosage, primary particle size and solid fraction) varied in turn away from a common baseline. Each run consisted of aggregate size measurements at a dozen different pipe lengths (mean residence times), giving a time profile for each set of conditions. Additional runs (runs #19 to 22) were performed in the gaps of the experimental matrix, by varying two of the process conditions simultaneously. The data from these runs were not used for model development or parameter estimation, but were used to test the predictive capability of the final model.

Model development

Aggregation

The population balance used here is based on the successful balance described by Hounslow et al.[62] and Spicer and Pratsinis[30]

$$\frac{dN_i}{dt} = \sum_{j=1}^{i-2} 2^{j-i+1}\alpha\beta_{i-1,j}N_{i-1}N_j + \frac{1}{2}\alpha\beta_{i-1,i-1}N_{i-1}^2 - N_i\sum_{j=1}^{i-1} 2^{j-i}\alpha\beta_{i,j}N_j - N_i\sum_{j=i}^{\infty}\alpha\beta_{i,j}N_j - S_iN_i + \sum_{j=i}^{\infty}\Gamma_{i,j}S_jN_j \quad (7)$$

The particle collision rate is given by the turbulent collision kernel of Saffman and Turner[1] (Eq. 3). Before flocculant addition, the primary particles are taken to be well dispersed as a stable suspension, although in many systems the primary particles may naturally coagulate to some extent due to a low-zeta potential. However, no large stable aggregates are formed at this stage, despite their collision in the turbulent flow. In the current system calcite particles are repelled by electrostatic repulsion,[17,63,64] and the effective capture efficiency (α) is taken to be zero. Alternatively, every collision could be considered to be successful ($\alpha = 1$), but with the breakage rate equal to the collision rate. Both methods were tried during model construction, but the former gave a simpler and more stable model and a better fit to the experimental data.

After the addition of flocculant, the aggregation rate exceeds the breakage rate, producing the increase in the aggregate size shown in Figure 1. In this case, the capture efficiency must be greater than zero, however, if the capture efficiency is set to unity immediately on flocculant addition, Eq. 3 considerably overestimates the aggregation rate compared to the experimental data. This is a common finding,[8,11,12,21,22,23,25,26,41,65-72] and the capture efficiency is frequently taken to be in the range 0.0001–0.5. In this case, if the capture efficiency was set to a constant value after flocculant addition, it had to be relatively small (~0.06) to give a reasonable fit to the data, suggesting that particle collision (Eq. 3) was not the rate-limiting step. Alternatively, the capture efficiency was taken to increase rapidly after flocculant addition (Eqs. 8 – 10), reflecting the mixing/adsorption time required for the polymer to reach the particle surface.

The mixing and adsorption behavior of polymer flocculants is complex and poorly described, although there is general agreement that adsorption is rapid under normal industrial conditions,[73-77] and that the bulk mixing of the flocculant and feed streams is rate limiting. This effect is likely to be highly scale-dependent, but its importance is evidenced by the com-

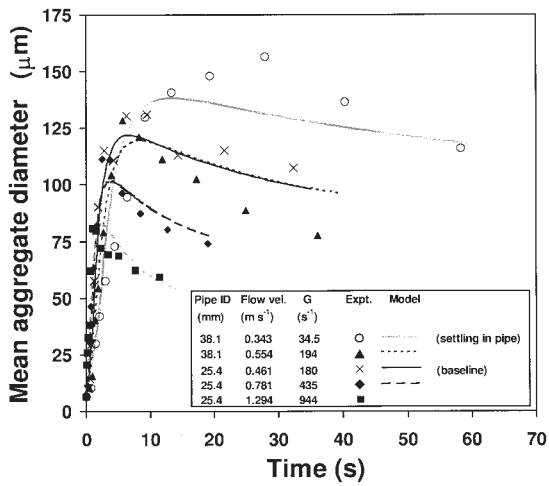

Figure 1. Modeled (lines) and experimental (dots) change in mean aggregate size under different pipe flow conditions.

At the lowest shear rate (open circles) solid settling was observed in the pipe, and these data should be interpreted with caution. Other conditions as per baseline.

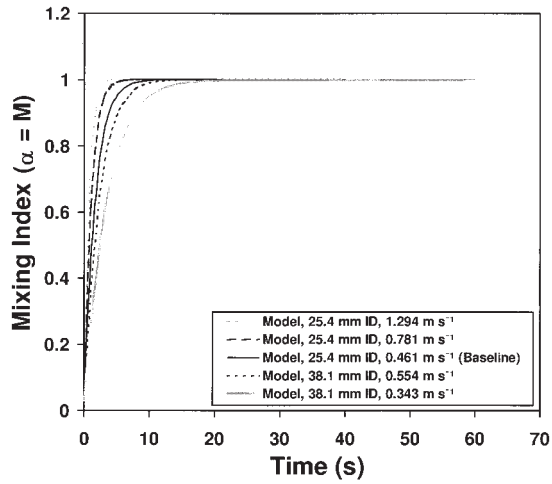

Figure 2. Variation in modeled mixing index with time under different flow conditions.

plexity of commercial feedwells, containing various design elements[78,79,80] to produce efficient flocculant mixing.

Mixing is usually described in terms of a mixing index[81,82,83]

$$M = 1 - \frac{\sigma}{\sigma_o} \tag{8}$$

However, experimental data for Eq. 8 is generally unavailable, and alternatively Etchells and Short[82] suggest for turbulent pipe flow

$$\frac{\sigma}{\sigma_o} = e^{-k_1\sqrt{fL/D}} \tag{9}$$

where k_1 = constant, ~ 0.5[82] (fitted parameter # 1); f = pipe friction factor (Eq. 13); L = pipe length, m; and D = pipe diameter, m.

Combining Eqs. 8 and 9 gives

$$\alpha \approx M = 1 - e^{-k_1\sqrt{fL/D}} \tag{10}$$

Equation 10 rapidly approaches unity (complete flocculant mixing/adsorption) by L $\sim$ 100 pipe dia. (Figure 2). The capture efficiency is also taken to approach unity at this point, independent of the flocculant dosage. In reality, the capture efficiency may never reach unity, and may vary as a function of the flocculant dosage.[36,37,38] However, the approach taken here was to make the population balance dosage dependent via the breakage kernels (next section, Eq. 21) reflecting an increase in aggregate strength with flocculant dosage.[84,85] Both approaches were tried during model construction, but making the breakage kernel (rather than the capture efficiency) dosage dependent gave a better fit with the experimental data.

Equation 10 is a reasonably crude approximation of the overall mixing/adsorption process and further work is required to better describe these effects. When the flocculant mixing/adsorption process is better understood it should be possible to further refine the capture efficiency term by including the effects of flocculant surface coverage and/or the hydrodynamic effect.

It would have been preferable to begin the experimental and model with the flocculant already well mixed, however, this is not possible with polymer flocculants. Studies of aggregation using salt coagulants can be performed[30] by adding coagulant to a stirred tank with a high-impeller speed to mix the coagulant and disperse the primary particles. The stirrer may then be turned down to give the appropriate shear rate and aggregation allowed to begin. However, this approach is not possible with fragile polymer flocculants and any initial rapid stirring results in irreversible polymer degradation.

Aggregation kernels for turbulent flow are usually written in terms of the mean shear rate (G)

$$G = \left(\frac{\varepsilon\rho_f}{\mu}\right)^{1/2} \tag{11}$$

The dissipation rate (ε) for turbulent pipe flow[79,86,87,88]

$$\varepsilon = \frac{2fV^3}{D} \tag{12}$$

and, for turbulent pipe flow in smooth pipes, the friction factor (f) is given by the Blasius[89] equation

$$f = \frac{0.0791}{\mathrm{Re}^{1/4}} \tag{13}$$

The slurry density (ρ_f) is readily calculated from experimental data given the solid fraction (ϕ) and the solid density (ρ_s)

$$\rho_f = \rho_s\phi + \rho_w(1 - \phi) \tag{14}$$

leaving the viscosity (μ) the only unknown in Eq. 11. The increase in fluid viscosity with solid fraction was described by Einstein[90] using the first terms of a series expansion in the form

$$\mu_s = \mu_o(1 + K_E\phi + \cdots) \tag{15}$$

where μ_s = viscosity of suspension, N s m^{-2}; μ_o = fluid viscosity (no solid), N s m^{-2}; K_E = constant = 2.5; and ϕ = solid fraction [0,1].

Equation 15 is only correct for very dilute solutions, and various alternative equations[87,91] have been proposed for higher solid fractions by adding additional terms.

For suspensions of very high-solid fraction the viscosity is typically given as a function of the maximum solid fraction in the form[87,91]

$$\mu_s = \mu_o\left(1 - \frac{\phi}{\phi_m}\right)^{-k} \tag{16}$$

where ϕ_m = maximum solid fraction; $k \approx 2$; μ_s = suspension viscosity, N s m^{-2}; μ_o = viscosity of water, 1.02×10^{-3} N s m^{-2} at 20 °C.

The maximum solid volume fraction is typically[92-95] taken as 0.6 – 0.7. At this point the particles are taken to be in close

contact and form a continuous network that resists shear, causing the viscosity to rise exponentially.

The effective solid fraction will be higher than the actual solid fraction because the aggregates are porous, incorporating fluid into the structure and increasing the enclosed volume, and, hence, the suspension viscosity.[32,96] The effective volume fraction (ϕ_{eff}) is described by fractal geometry[24,55,68,96,97]

$$\phi_{eff} = \phi\left(\frac{\rho_s}{\rho_{agg}}\right) \tag{17}$$

where ϕ_s = actual suspension solid volume fraction [0,1]; ρ = density of the solid, calcite = 2710 kg m^{-3}; and ρ_{agg} = effective aggregate density (kg m^{-3}), given by

$$\rho_{agg} = \rho_s\left(\frac{d_{agg}}{d_p}\right)^{D_f-3} \tag{18}$$

where d_{agg} = diameter of aggregate, m; d_p = primary particle diameter, m; and D_f = mass-diameter fractal dimension. Substituting and using mean sizes gives

$$\mu_s = \mu_0\left(1 - \frac{\phi_{eff}}{\phi_m}\left(\frac{\overline{d_{agg}}}{\overline{d_p}}\right)^{3-D_f}\right)^{-k} \tag{19}$$

In this case the maximum packing fraction (ϕ_m = 0.65) and exponent (k = 2) are effectively model parameters estimated from the literature. During model construction ϕ_m was initially treated as a fitted parameter [0.6, 0.7], however, the model was surprisingly insensitive to ϕ_m over that range, and was subsequently fixed at an intermediate value of 0.65, removing a degree of freedom. The fractal dimension (2.4) was estimated from the hindered settling data and will be discussed in a future article.

Aggregate breakage

Aggregate breakage is described by the final two terms in the population balance (Eq. 7). Breakage is taken to be binary, producing two equal sized daughter fragments, which is a common modeling approach.[3,24,30,42,43] In the case of the population balance used here (Eq. 7), the method of discretization is relatively coarse with the aggregate mass doubling every channel[62] in an effort to reduce the number of size fractions and equations. Because of this, most of the particles in a distributed breakage function[30] will naturally appear in the next smallest size range anyway, unless the distribution is very broad, or the number of fragments is assumed to be > 2. In the case of a broad distribution, problems may arise unless the distribution is truncated so that the daughter fragments must be smaller than the parent aggregate.

Equation 6 suggests (note Eq. 11) that the breakage rate is decreased as a function of viscosity, although some workers have suggested the more intuitive response that the breakage will increase with the viscosity.[41,58] In most cases the form of Eq. 6 has been successful, because most previous studies have focused on coagulation in water treatment plants or river estuaries which are characterized by a low-solid fraction, where the viscosity is essentially unchanged from pure water.[24,29,30,98,99,100]

However, feedstreams to thickener units used in mineral processing have a considerably higher solid volume fraction, typically in the percent range.[78,79,101] Hence, in this case the breakage rate was initially considered to be $\propto \varepsilon^n\mu^z$ where μ, the viscosity, is given by Eq. 19. During model construction, parameter estimation (see next section) repeatedly gave n = 0.7 ± 0.1, and z = 1 ± 0.05. The value of ~ 0.7 is similar to other studies,[29,30,56] while z was set to unity, removing a degree of freedom from the model.

Flocculant dosage dependency is also introduced into the breakage kernel to account for the formation of larger aggregates at higher dosages (Figure 8). The dosage is expressed as a surface coverage (θ_f) on a mass/area basis calculated from the experimental addition rate and measured particle surface area

$$\theta_f = \frac{m_f}{A_s}M(1 - \Theta) \tag{20}$$

and the breakage kernel is

$$S_i = \frac{k_2\varepsilon^{k_3}\mu d_{agg,i}}{\theta_f} \qquad d_{agg} > d_p = 0 \qquad d_{agg} \le d_p \tag{21}$$

where θ_f = effective flocculant surface coverage, kg m^{-2}; k_2 = fitted parameter # 2; k_3 = fitted parameter # 3; M = mixing index given by Eq. 10; m_f = mass of flocculant, kg; A_s = surface area of solid, m^2; and Θ = flocculant degradation [0,1] (Eq. 22).

Studies of coagulation typically show an initial increase in the aggregate size after coagulant addition, followed by the attainment of a stable steady-state size.[24,29,30,55] However, polymer flocculants do not give a steady-state size except if flocculation occurs primarily through surface charge neutralization. Aggregation by polymer bridging typically results in a decreased aggregate size on extended shearing due to flocculant degradation through carbon chain scission or rearrangement.[54,74,102,103,104,105]

Polymer flocculant degradation can be incorporated into the model with a decreasing capture efficiency,[106] or by an increased breakage rate via a weaker aggregate. The latter approach was taken here, keeping the terms together in the breakage kernel

$$\frac{d\Theta}{dt} = k_4\varepsilon^{k_3}\mu\phi M\left(1 - \Theta\left(\frac{\phi_{eff}}{\phi}\right)^{1/3}\right) \tag{22}$$

Initially the flocculant degradation is zero, that is, $\Theta = 0$ at $t = 0$.

The rate of polymer degradation is taken to be a function of the breakage rate, although additional solid fraction dependence was required to achieve an acceptable fit with the data. The dimensionless term $(\phi_{\text{eff}}/\phi)^{1/3}$ is introduced to prevent the polymer becoming completely degraded. The term can be replaced by ≈ 2 (allowing 50% degradation) giving only a slight increase in the residual. However, the term used has the additional advantage that it collapses to 1 (complete degradation) under unfavorable conditions (that is, extreme shear),

allowing the aggregate-size distribution to eventually return to the primary particle size.

The physical interpretation of this effect is not clear, and could be taken as evidence of flocculation by surface charge neutralization. However, in this case an anionic polymer was used and the calcite surface is predominantly negatively charged.[107] Adsorption is via the neutrally charged amide groups on the polymer and the neutral sites on the particle surface. Alternatively, the effect could be taken as evidence that the flocculant binding together the core of aggregates is not significantly degraded, because the aggregates are not broken down to that extent. The polymer degradation would then be expected to be a function of the aggregate surface area, volume, packing efficiency, and so on. The term used is entirely empirical at this stage, although it is in a similar form to that used by Strenge[93] to describe the mean distance between particles in the aggregate.

Fitting the model to experimental data

The population balance model described above contains 4 fitted parameters (Eqs. 10, 21 and 22) that are estimated from the experimental size data[60] using a conventional sum-of-squares minimization

$$\min_{k_1,k_2,k_3,k_4} \psi = \sum_{G,\phi,d_p,\theta,t} (\bar{d}_{agg,\mathrm{PB}} - \bar{d}_{agg,\mathrm{Exp}})^2 \tag{23}$$

Where k_n = fitted parameters; G = spatially averaged shear rate, s^{-1}; ϕ = solid fraction, $m^3\ m^{-3}$; θ = flocculant surface coverage, kg m^{-2}; d_p = primary particle size, m; $d_{agg,\mathrm{PB}}$ = modeled (PB = population balance) mean aggregate size, m; $d_{agg,Exp}$ = experimental (FBRM) mean aggregate size, m; and t = time, s.

The population balance models the aggregate-size distribution through time. From this the volume-weighted mean aggregate diameter is calculated by

$$\overline{d_{agg}} = \frac{\Sigma_i N_i d_i^4}{\Sigma_i N_i d_i^3} \tag{24}$$

The predicted mean sizes are then compared to the experimental results at the corresponding time instants for each of the pipe reactor runs (Eq. 23), with the parameters varied to give the best fit.

Simulations and parameter estimation were performed using gPROMS®, a commercial UNIX® based dynamic simulation package, running on a SUN Enterprise 3,000 mainframe. Individual simulations took in the order of 10 s to run, while parameter estimation using the 17 available data sets took several hours.

The fitted parameters are used to fit the model to the experimental data, with the parameters adjusting various aspects of the model behavior. The first parameter (k_1) alters the initial flocculant/suspension mixing rate in the pipe, changing the capture efficiency and hence the initial rate of aggregation. The fitted value of 0.343 compares favorably with the literature[82] value of 0.5. However, in its current form the mixing equation (Eq. 10) only describes mixing in turbulent pipe flow, and requires modification for other systems.

Table 2. Matrix of Pipe Reactor Experimental Results

Run No.	Viscosity (N s m^{-2})	Susp. Density (kg m^{-3})	Re	ε ($m^2\ s^{-3}$)	G (s^{-1})	f
1	0.0024	1063	5291	0.071	180	0.0093
2	*0.0165*	*1063*	*752*	*0.116*	*86*	*0.0151*
3	0.0016	*1063*	*7681*	*0.065*	*207*	*0.0084*
4	*0.0509*	*1063*	*245*	*0.154*	*57*	*0.0200*
5	0.0014	1063	8759	0.063	217	0.0082
6	0.0018	1042	6821	0.067	198	0.0087
7	0.0030	1105	4294	0.075	166	0.0098
8	0.0015	1021	8222	0.064	212	0.0083
9	0.0027	1084	4637	0.074	171	0.0096
10	0.0015	1063	13700	0.274	435	0.0073
11	0.0012	1063	28173	1.039	944	0.0061
12	0.0019	1063	11736	0.068	194	0.0076
13	*0.0330*	*1063*	*421*	*0.037*	*34*	*0.0174*
14	*0.1675*	*1063*	*50*	*0.014*	*9*	*0.0297*
15	0.0058	1063	2158	0.089	128	0.0116
16	0.0019	1063	6478	0.068	194	0.0088
17	0.0016	1063	7996	0.064	210	0.0084
18	*0.0101*	*1063*	*1237*	*0.103*	*104*	*0.0133*
19	0.0028	1042	4307	0.075	166	0.0098
20	0.0012	1063	16934	0.260	471	0.0069
21	0.0029	1063	4715	0.020	85	0.0095
22	*0.0136*	*1042*	*1000*	*0.030*	*48*	*0.0140*

The second model parameter (k_2) scales the breakage rate, and is likely to be a complex function of the various factors affecting the aggregate strength. For example, the flocculant/particle surface bonding chemistry, the flocculant molecular weight, the presence of coagulating salts (if any), or the primary particle packing structure within the aggregate.

The third fitted parameter (k_3) alters the effect of the energy dissipation rate on the final aggregate size, producing a smaller aggregate at higher shear rates as described above. The final parameter (k_4) sets the rate of polymer degradation at extended residence times. Due to the complex interrelated nature of the population balance equations and the fact that aggregation and breakage occur simultaneously the parameters are somewhat interactive, with any deficiencies in the model effectively accommodated elsewhere in the model. However, the model was found to be robust, converging to the same parameter values from a range of initial estimates.

Comparison with Experimental Data

Effect of flow regime (shear rate)

Figure 1 compares the modeled and experimental[60] mean aggregate size data for calcite under various flow conditions. A combination of pipe sizes (25.4 or 38.1 mm ID) and flow rates gave different fluid shear rates. A higher mean fluid shear results in a rapid initial aggregation rate, but ultimately leads to a smaller mean aggregate size due to increased breakage. The population balance model (lines) follows the same trends due to the interplay between various factors. At a higher shear rate the flocculant mixing (Eq. 10, Figure 2) and particle collision (Eq. 3) rates are higher, resulting in a higher initial aggregation rate. However, a higher energy dissipation rate also increases the breakage (Eq. 21) and polymer degradation (Eq. 22) rates, resulting in a smaller average aggregate size later in the reaction.

Table 2 shows a summary of the experimental results for viscosity, mean shear rate, friction factor, pipe Reynolds num-

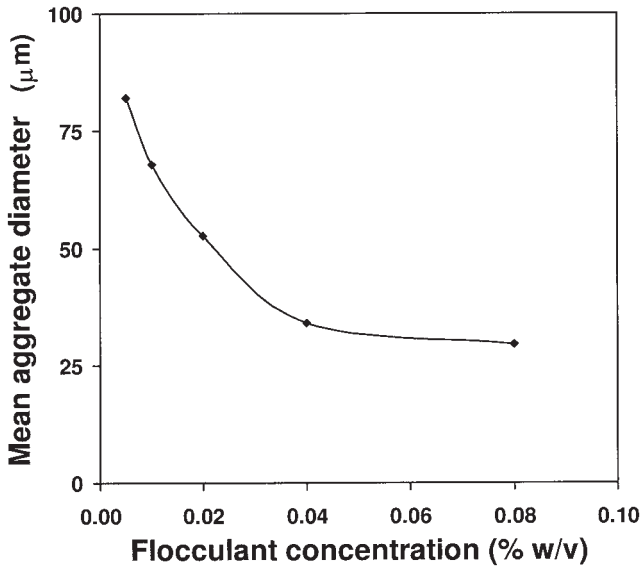

Figure 3. Effect of flocculant stream dilution on the measured aggregate size for a fixed (short) length of pipe, giving a mean residence time of 3 s, see Figure 1: 38.1 mm ID pipe, 0.34 m s^{-1} mean flow velocity.

ber, and so on, for all of the experimental runs, as outlined in Table 1, with the corresponding aggregate size data described in subsequent sections. In some cases the aggregated suspensions were observed to stratify/settle in the pipe reactor, leading to uncertainties in the solid fraction and average residence time, correspondingly shown in italics in Table 2, and these results should be interpreted with caution.

Figure 2 shows the modeled flocculant/suspension mixing index (M, Eq. 10) as a function of time and the flow regime, allowing an estimation of the capture efficiency (α), which is also taken to approach 1 when the flocculant becomes well mixed. The actual capture efficiency may be lower than 1, although the real value is unknown and any discrepancy is effectively compensated by the breakage kernel.

Figures 1 and 2 suggest that the initial aggregation rate is limited by flocculant/suspension mixing, rather than the particle collision rate (Eq. 3). This is supported by experimental evidence where the mixing was changed, either by flocculant dilution or by changing the flocculant injection velocity by changing the injection nipple size. Figure 3 shows the increase in the aggregate size with flocculant dilution with a fixed length of short pipe (1 m) (compare Figure 1, 38.1 mm ID, 0.55 m s^{-1}). Using a short length of pipe and gentle shear rate allowed the particle size measurement to be taken where the aggregate size was still increasing rapidly and was likely to be influenced by the mixing condition. The overall dosage was maintained at 20 g t^{-1}, but a dilute flocculant stream produced better mixing due to a higher flocculant stream flow, and lower viscosity.

Increasing the flocculant injection velocity by changing the inlet nipple diameter (not shown) gave a similar result, with a smaller inlet nipple increasing the flocculant stream momentum, the turbulence at the injection point, producing an increased aggregate size at short residence times. In all cases the flocculant stream was minor (0.25–2%) compared to the main slurry flow in the pipe reactor.

Figure 4 shows the variation in the modeled fluid viscosity under the conditions described by Figure 1. The fluid viscosity (Eq. 19) is taken to be a function of the effective solid fraction (Eq. 16), including aggregate porosity using fractal geometry. Since aggregates become increasingly porous as they increase in size, the total enclosed volume of the aggregates also increases, leading to a higher effective solid fraction, and, hence, fluid viscosity.[104,108] This effectively prevents gelation, where the aggregates might grow to the point where they fill the container, because as the effective solid fraction approaches the maximum (ϕ_m), the viscosity tends toward infinity (Eq. 19). This leads to an increased pressure drop (as measured by the manometer), and an increased energy dissipation rate (the flow velocity is fixed via a positive displacement pump), and hence an increased breakage rate (Equation 21).

Since the fluid viscosity (Figure 4) is dependent on the aggregate size, various other fluid parameters (shear rate, friction factor, Reynolds number) also change and are calculated within the population balance. The use of manometers during the experimental[60] allowed experimental estimates of the same fluid properties, with the predicted and experimental average shear rates compared in Figure 5. These fluid parameters are described using standard pipe flow equations (Eqs. 12–13) incorporating the effect of solid fraction on the suspension viscosity (Eqs. 16–19), achieving an acceptable fit to the data (Figure 5) without the need for any additional fitted parameters.

Figure 6 shows the population balance correctly conserved mass through time according to

$$\phi_t = \sum_i \frac{N_i m_i}{\rho_s} \tag{25}$$

where ρ_s = density of the solid, 2710 kg m^{-3}; m_i = mass of i^{th} aggregate, kg; and N_i = number of i^{th} aggregates, m^{-3}. Although conservation of mass does not guarantee that the pop-

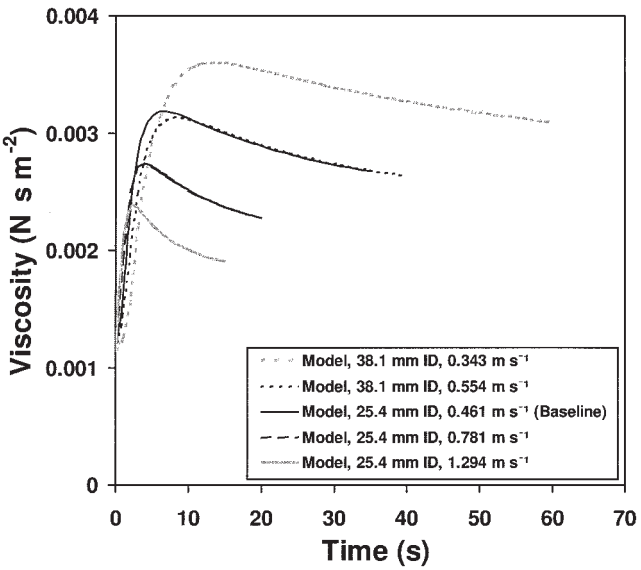

Figure 4. Variation in the modeled fluid viscosity under different flow regimes: other conditions as per baseline.

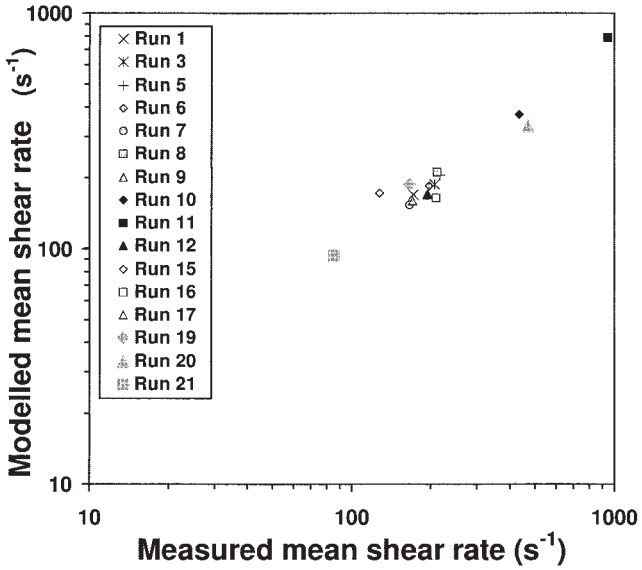

Figure 5. Comparison between modeled and experimental spatially averaged shear rates.

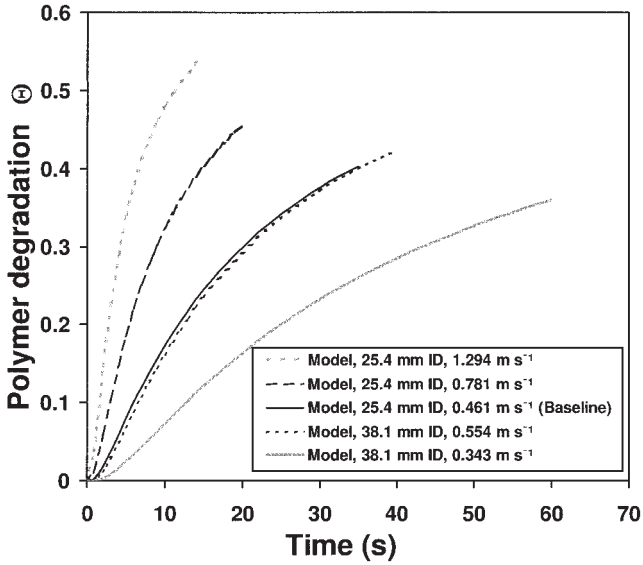

Figure 7. Variation in the modeled polymer deactivation index under different flow regimes.

ulation balance is working correctly, it is simple to check and picks up gross coding and numerical errors that frequently result in the model gaining or losing mass.

Aggregation with polymer flocculant typically results in partially irreversible breakage, manifesting as a gentle reduction in the aggregate size after an initial peak as the polymer becomes degraded.[74] Figure 7 shows the extent of flocculant degradation predicted by the model under various flow conditions. Due to the incorporation of the $(\phi_{eff}/\phi_s)^{1/3}$ term in Eq. 22, the degradation tends toward a value of less than 1 (where 1 would represent complete degradation). This improves the fit with the experimental data, and is rationalized on the basis that the repeated aggregation/breakage process will not affect flocculant binding the core of aggregates, because the aggregates are not broken down to that extent. However, if the flow conditions are very aggressive, aggregation will only proceed to a limited extent and $\phi_{eff} \rightarrow \phi_s$, therefore, the flocculant could be completely degraded. Such a situation is clearly undesirable industrially, but may occur around feed entry points or baffles with high-local shear rates.

Effect of flocculant dosage

Figure 8 shows the predicted and experimental mean aggregate sizes as a function of time and flocculant dosage. The

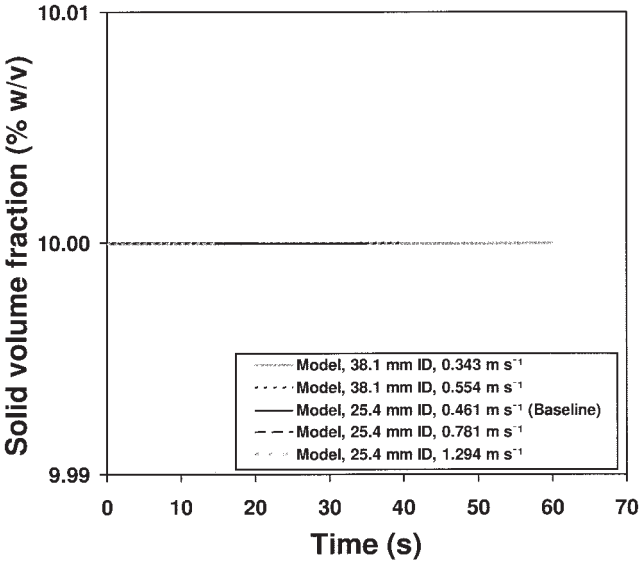

Figure 6. Variation in the modeled absolute mass fraction under different flow regimes: conservation of mass.

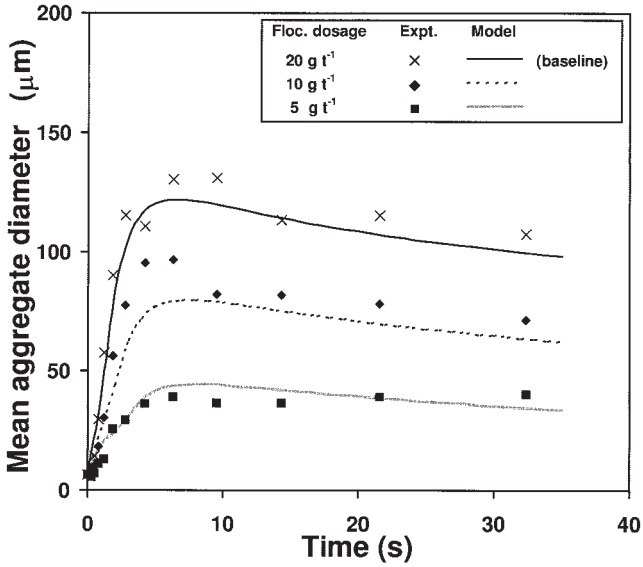

Figure 8. Modeled (lines) and experimental (dots) change in mean aggregate size with change in flocculant dosage: other conditions as per baseline.

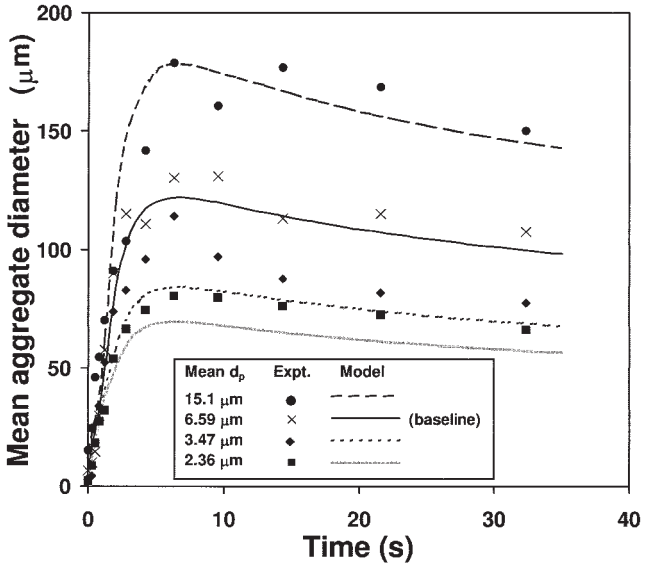

Figure 9. Modeled (lines) and experimental (dots) change in mean aggregate size using differently sized primary particles: other conditions as per baseline.

dosage does not affect the aggregation term in the population balance and the capture efficiency is taken to approach 1 as the flocculant/suspension mixing becomes complete, regardless of the actual flocculant dosage. However, flocculant dosage is incorporated into the breakage kernel of the population balance (Eq. 21), where a higher dosage leads to a stronger aggregate, a decreased breakage rate, and, hence, larger aggregates. The flocculant dosage is known experimentally on a mass basis, but is incorporated into the population balance as a surface coverage, that is, kg (floccuant) per m^2 (solid) (Eq. 20). The surface area of the primary particles was calculated from the particle size measured by laser diffraction (Malvern Mastersizer) since this was more likely representation of the area assessable to flocculant than that determined by BET (which includes internal pore related surface area). Hence, the effective surface coverage also depends on the primary particle size (Figure 9).

Higher dosages were also tried, but resulted in stratification/settling in the pipe reactor, leading to uncertainty in the solid fraction and residence time. Both the model and experimental results gave larger aggregates at higher dosages, although the data match was poor (not shown). At extremely high-flocculant dosages there is data to suggest[80,92,109] that the aggregate size can be reduced by steric restabilization as the particle surface becomes completely covered, although it is unlikely that such a high dosage would be reached in industrial applications.[105]

Effect of primary particle size

The primary particle-size distribution is also likely to be a process variable, depending on the feed (milling, crystallization, ore, for example). This effect was incorporated into the population balance model by assuming that the aggregate breakage rate is a function (Eq. 21) of the effective flocculant surface coverage. That is, a larger primary particle, with a smaller effective surface area (per unit mass) has a higher coverage, a higher strength, and, hence, results in larger aggregates (Figure 9).

Figure 9 shows that using the effective flocculant dosage gives the correct model response with respect to primary particle size, although the modeled size underestimates the experimental data for small primary particles. An alternative particle surface area measurement (BET) was also tried, giving similar results, but no improvement in the fit. Although the discrepancy is clearly noticeable to the eye, the residual error is comparatively minor and did not justify the addition of a further fitted parameter.

Alternatively, the aggregate strength could be considered to be a function of the packing efficiency within the aggregate,[17,75] which would change with primary particle size according to Eq. 18. Attempts were made along these lines during model construction, but ultimately did not fit the experimental data as well as relating the aggregate strength to the flocculant surface coverage. The latter also gave a simpler model.

Effect of solid fraction

The solid fraction is also a process variable and can be altered in some processes by overflow or underflow recycle.[79] Figure 10 shows a comparison between model and experimental mean aggregate sizes as a function of time and solid fraction. The reduction in aggregate size with solid fraction might be somewhat unexpected, given that aggregation (Eq. 4) is usually taken as second-order with respect to particle number, whereas breakage is taken as first-order (Eq. 5). However, by making the modeled breakage rate a function of viscosity (Figure 11) and the energy dissipation rate (which also increases with the viscosity; Equations 16–19), the breakage rate was increased at high-solid fraction, producing the desired reduction in the aggregate size (Figure 10). In addition, an increased solid fraction gives a reduced shear rate further reducing the aggregation rate. At relatively high-solids concen-

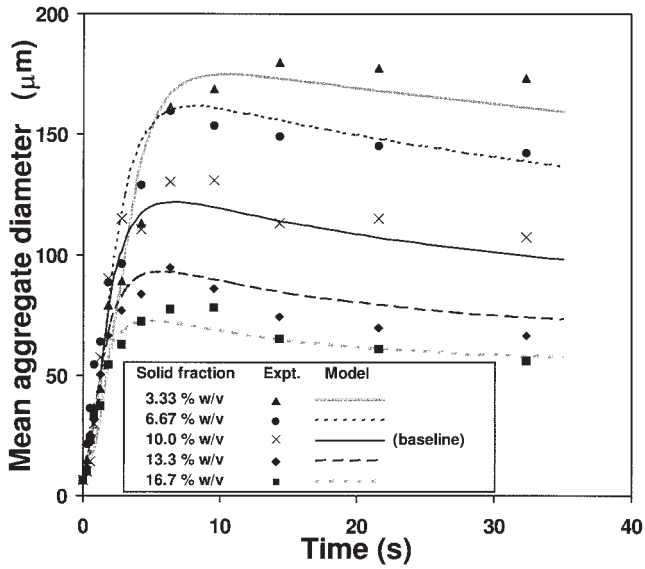

Figure 10. Modeled (lines) and experimental (dots) change in mean aggregate size using different solid fractions: other conditions as per baseline.

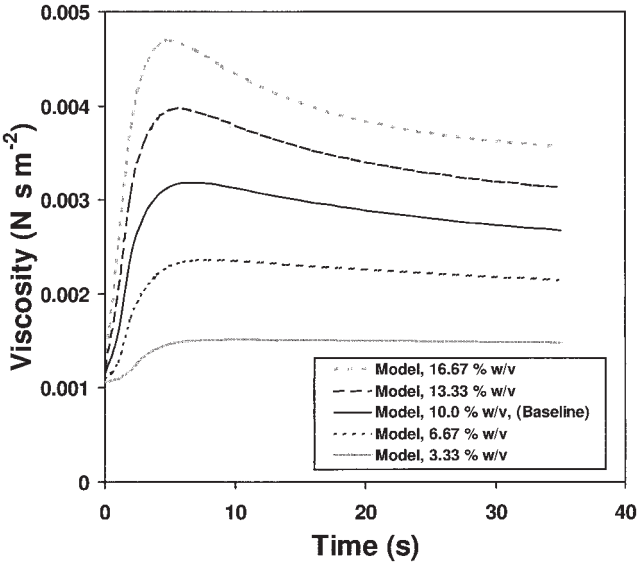

Figure 11. Variation in modeled fluid viscosity through time with various solid fractions.

trations a reduction in aggregate size with increased solid fraction has been observed elsewhere.[40,104]

At very low-solid fraction (< 3% w/v), the viscosity approaches that of pure water, and the model predicts a reduction in aggregate size as the solid fraction is further decreased due to the difference in the order of the aggregation and breakage kernels. The increase in aggregate size with increased solid fraction has been observed previously in studies at very low-solid fraction.[10,110,111] Lower solid fractions were not investigated here due to the difficulty of measuring the hindered settling velocity (the subject of a latter article) at low-solid fraction where the mudline is no longer distinct, and the settling rate is rapid.

Additional runs to check model predictive capability

Figures 1, 8, 9 and 10 show results from a sparse matrix of experimental pipe reactor runs performed using the baseline as the central point, and varying the process variables (fluid shear, flocculant dosage, solid fraction, primary particle size) independently away from that the center. However, additional experimental runs were performed in the gaps of the matrix, by changing two process variables simultaneously. These were not included in the parameter estimation for the population balance, but were used to assess the predictive capability of the model (Figure 12). The predictions appear reasonable, except for the latter stages of the 15.1 μm, 6.67% w/v run. This appears to be due to the effect of the primary particle size, which shows some deviation from the experimental values (see Figure 9).

Conclusions

A population balance model has been developed to describe the kinetics of aggregation/breakage of calcite particles flocculated with high-molecular-weight flocculant in turbulent flow. In addition to the effect of fluid shear normally incorporated into population balance models of aggregation, the model accounts for the important full-scale process variables, namely: flocculant dosage, primary particle size and solid fraction, representing a significant advance on the population balance models that have been described in the literature.

The population balance is based on the successful model proposed by Hounslow et al.[62], later modified to incorporate aggregate breakage by Spicer and Pratsinis.[30] Saffman and Turner's[1] collision kernel is used in conjunction with a capture efficiency (α) term, based on the degree of flocculant/suspension mixing. This accounts for the stability of the suspension before flocculant addition, and prevents the overestimation of the aggregation rate during the initial mixing period.

The breakage kernel is a function of the mean energy dissipation rate, suspension viscosity and aggregate diameter. Flocculant dosage dependence is also incorporated into the breakage term, with a higher dosage increasing the aggregate strength, leading to a reduced breakage rate and ultimately a larger aggregate size. The partial nonreversibility of polymer aggregate breakage is included with a decay term that accounts for the flocculant degradation due to repeated aggregation/breakage.

The effects of aggregate porosity are incorporated by the use of fractal geometry, increasing both the effective capture radii and the effective solid fraction. The increase in the suspension viscosity with solid volume fraction is also incorporated, and results in changes in the energy dissipation rate, fluid shear, pipe friction factor and Reynolds number. The inclusion of these additional terms allow the population balance to describe aggregation and breakage kinetics in suspensions of high-solid fraction as found in mineral processing thickeners.

Acknowledgments

This research has been supported by the Australian Government's Cooperative Research Centre (CRC) program, through the AJ Parker CRC for Hydrometallurgy. Support was also provided by the AMIRA P266C Im-

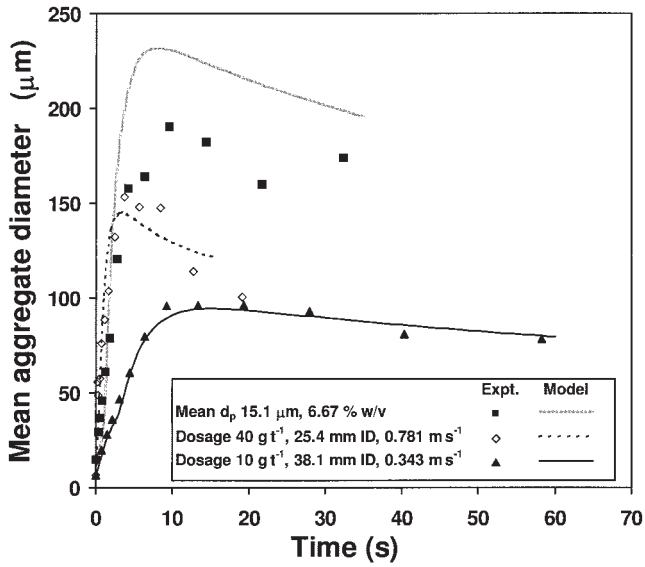

Figure 12. Modeled (lines) and experimental (dots) change in mean aggregate size with change under various additional conditions: other conditions as per baseline.

proving Thickener Technology project. This support is gratefully acknowledged.

Notation

A_s = surface area of solid, m^2
a_i = radius of i^{th} particle, m
D = pipe diameter, m
D_f = mass-diameter fractal dimension
d_{agg} = diameter of aggregate, m
$d_{agg,Exp}$ = experimental (FBRM) mean aggregate diameter, m
$d_{agg,PB}$ = modeled (PB = population balance) mean aggregate diameter, m
d_p = primary particle diameter, m
f = pipe friction factor, dimensionless
G = spatially averaged mean shear rate, s^{-1}
$k \approx 2$, Eq. 16, dimensionless
k_1 = fitted parameter # 1 = 0.3431
k_2 = fitted parameter # 2 = 38.1
k_3 = fitted parameter # 3 = 0.677
k_4 = fitted parameter # 4 = 1224
K_E = Einstein's constant = 2.5
L = pipe length, m
M = mixing index, [0,1]
m_f = mass of flocculant, kg
m_i = mass of i^{th} aggregate, kg
N_i = number of i^{th} particles or aggregates, m^{-3}
Re = Reynolds number, dimensionless
S_k = breakage rate (kernel) of k^{th} sized particles, s^{-1}
t = time, s
V = velocity, m s^{-1}

Greek letters

α = collision capture efficiency (# collisions resulting in aggregation/ Tot. # collisions), [0,1]
β_{ij} = rate of collision between i and j sized particles (aggregation kernel), m^3s^{-1}
ε = local turbulent energy dissipation rate per unit mass, m^2s^{-3}
ϕ = solid volume fraction, [0,1]
ϕ_{eff} = effective volume fraction, including aggregate porosity [0,1]
ϕ_m = maximum solid fraction
ρ_s = density of the solid, calcite = 2710 kg m^{-3}
ρ_f = suspension density, kg m^{-3}
ρ_{agg} = aggregate density, kg m^{-3}
ρ_w = density of liquid phase, water, kg m^{-3}
μ = viscosity, N s m^{-2}
μ_s = suspension viscosity, N s m^{-2}
μ_o = fluid viscosity (no solid), N s m^{-2}
Γ_{lk} = Breakage distribution function (number of k size particles produced from the breakage of a l sized particle)
θ_f = effective flocculant surface coverage, kg m^{-2}
σ = concentration variation
σ_o = initial concentration variation
γ = laminar shear rate, s^{-1}
ν = kinematic viscosity, m^2s^{-1}
λ = characteristic wavelength, m
Φ = energy dissipation rate per unit volume, kg $m^{-1}s^{-3}$
Θ = flocculant degradation [0,1]

Literature Cited

1. Saffman P, Turner J. On the collision of drops in turbulent clouds. *J of Fluid Mech.* 1956;1:16-30.
2. Friedlander SK. *Smoke, Dust, and Haze*. New York: Wiley; 1977.
3. Randolph AD, Larson MA. *Theory of Particulate Processes*, 2nd ed. NY: Academic Press; 1988.
4. Sonntag RC. Coagulation kinetics. In: Dobias B. *Coagulation and flocculation: Theory and applications*. USA: Marcel Dekker; 1993.
5. Shamlou PA, Titchener-Hooker N. Aggregate behaviour in stirred vessels. In: Shamlou, PA. *Processing of Solid-Liquid Separations.* UK: Butterworth-Heinemann; 1993.
6. Smoluchowski M. Drei Vortrage uber diffusion brownsche bewegung und koagulation vol kolloidteilchen. *Physick Zeitschrift*. 1916; 17:557.
7. Smoluchowski M. Versuch einer mathematischen theorie der koagulationskinetic kolloider lösungen. *Z Phys Chem*. 1917;92:129-168.
8. Tambo N, Watanabe Y. Physical aspects of flocculation process: I. Fundamental treatise. *Water Res*. 1979;13:429-439.
9. Wagberg L, Lindstroem T. Kinetics of polymer induced flocculation of cellulosic fibres in turbulent flow. *Colloids Surfaces.* 1987;27:29-42.
10. de Boer GBJ, Hoedemakers GFM. Thoenes D. Coagulation in turbulent flow: part I. *Chem Eng Res Des*. 1989;67:301-307.
11. de Boer GBJ, Hoedemakers GFM, Thoenes D. Coagulation in turbulent flow: part II. *Chem Eng Res Des*. 1989;67:308-315.
12. Brunk PB, Kock DL, Lion LW. Turbulent coagulation of particles. *J of Fluid Mechanics*. 1998;364:81-113.
13. Camp TR, Stein PG. Velocity gradients and internal work in fluid motion. *J Boston Soc Civ Eng*. 1943;20:219 -237.
14. Clark MM. Critique of Camp and Stein's RMS velocity gradient. *J Env Eng*. 1985;111:741-754.
15. Cleasby JL. Is velocity gradient a valid turbulent flocculation parameter? *J Env Eng*. 1984;110:875-987.
16. Spielman LA. 'Hydrodynamic aspects of flocculation' In: Ives KJ. *The Scientific Basis of Flocculation*. The Netherlands: Sijthoff and Noordhoff; 1978;207-233.
17. Gregory J. Fundamentals of flocculation. *CRC Critical Reviews in Environ Cont*. 1989;19:185-230.
18. Kuboi R, Komasawa I, Otake T. Collision and coalescence of dispersed drops in turbulent liquid flow. *J of Chem Eng of Japan*. 1972;5:97-98.
19. Delichatsios MA, Probstein RF. Coagulation in turbulent flow: theory and experiment. *J of Colloid Interface Sci*. 1975;51:394-405.
20. Swift DL, Friedlander SK. The coagulation of hydrosols by Brownian motion and laminar shear flow *J of Colloid Interface Sci*. 1964;19: 621-647.
21. Burban P, Lick W, Lick J. The flocculation of fine-grained sediments in estuarine waters. *J Geophys Res*. 1989;94:8323-8330.
22. Chin CJ, Yiacoumi S, Tsouris C. Shear-induced flocculation of colloidal particles in stirred tanks. *J of Colloid and Interface Sci*. 1998;206:532-545.
23. Ducoste JJ, Clark MM. The influence of tank size and impeller geometry on turbulent flocculation: II. Model. *Environ Eng Sci*. 1998;15:225-235.
24. Flesch JC, Spicer PT, Pratsinis SE. Laminar and turbulent shear-induced flocculation of fractal aggregates. *AIChE J*. 1999;45:1114-1124.
25. Gonzalez EA, Hill PS. A method for estimating the flocculation time of monodispersed sediment suspensions. *Deep-Sea Res*. 1998;45: 1931-1954.
26. Han MY, Lawler DF. The (relative) insignificance of G in flocculation. *J of the A Water Works Assoc*. 1992;84:79-91.
27. Higashitani K, Yamauchi K, Matsuno Y, Hosokawa G. Turbulent coagulation of particles in a viscous fluid. *J Chem Eng Japan*. 1983;16:299-304.
28. ∅degaard H. Orthkinetic flocculation of phosphate precipitates in a multicompartment reactor with non-ideal flow. *Prog Wat Tech*. 1979; 1:61-68.
29. Serra T, Casamitjana X. Modelling the aggregation and break-up of fractal aggregates in a shear flow. *Appl Sci Res.* 1998;59:255-268.
30. Spicer PT, Pratsinis SE. Coagulation and fragmentation: Universal steady-state particle-size distribution. *AIChE J*. 1996;42:1612-1620.
31. van de Ven TGM, Mason SG. The microrheology of colloidal dispersions VII. Orthokinetic doublet formation of spheres. *Colloid Polym Sci*. 1977;255:468-479.
32. Potanin AA, Uriev NB. Microrheological models of aggregated suspensions in shear flow. *J of Colloid Interface Sci*. 1991;142:385-395.
33. Adachi Y, Stuart MAC, Fokkink R. Kinetics of turbulent coagulation studied by means of end-over-end rotation. *J of Colloid Interface Sci*. 1994;165:310-317.
34. Deryagin BV, Landau LD. Theory of the stability of strongly charged lyophobic sols and the adhesion of strongly charged particles in solutions of electrolytes. *Acta Physicochimica URSS*. 1941;14:633-662.
35. Verwey EJW, Overbeek JTG. *Theory of the stability of lyophobic colloids* Amsterdam: Elsevier; 1948.

36. Healy TW, La Mer VK. The energetics of flocculation and redespersion by polymers. *J of Colloid Sci*. 1964;19:323-331.
37. Hogg R. Collision efficiency factors for polymer flocculation. *J of Colloid Interface Sci*. 1984;102:232-236.
38. Hsu J-P, Lin D-P, Tseng S. The sticking probability of colloidal particles in polymer-induced flocculation. *Colloid Polym Sci*. 1995; 273:271-278.
39. Argaman Y, Kaufman WJ. Turbulence in orthokinetic flocculation. *SERL Report No. 68-5*. Berkeley: Sanitary Engineering Research Laboratory, University of California; 1968.
40. Lick W, Lick J. Aggregation and disaggregation of fine-grained lake sediments. *J Great Lakes Res.* 1988;14:514-523.
41. Kramer TA, Clark MM. Incorporation of aggregate breakup in the simulation of orthokinetic coagulation. *J of Colloid and Interface Sci*. 1999;216:116-126.
42. Chen W, Fisher RR, Berg JC. Simulation of particle size distribution in an aggregation-breakup process. *Chem Eng Sci*. 1990;45:3003-3006.
43. Chatzi EG, Kiparissides C. Steady-state drop-size in high holdup fraction dispersion systems. *AIChE J.* 1995;41:1640-1652.
44. Valentas KJ, Amundson NR. Breakage and coalescence in dispersed phase systems. *Ind Eng Chem Fundam*. 1966;5:533-542.
45. Valentas KJ, Gilous O, Amundson NR. Analysis of breakage in dispersed phase systems. *Ind Eng Chem Fundam*. 1966;5:271-279.
46. Coulaloglou CA, Tavlarides LL. Description of interaction processes in agitated liquid-liquid dispersions. *Chem Eng Sci*. 1977;32:1289-1297.
47. Lu CF, Spielman LA. Kinetics of floc breakage and aggregation in agitated liquid suspensions. *J of Colloid and Interface Sci*. 1985;103: 95-105.
48. Cheng Z, Redner S. Scaling theory of Fragmentation. *Physical Review Letts*. 1988;60:2450-2453.
49. Burban P, Lick W, Lick J. The flocculation of fine-grained sediments in estuarine waters. *J Geophys. Res*. 1989;94:8323-8330.
50. Parker DS, Kaufman WJ, Jenkins D. Floc breakup in turbulent flocculation processes. *Sanitary Eng Div*. 1972;8702:79-99.
51. Lee CW, Brodkey RS. A visual study of pulp floc dispersion mechanisms. *AIChE J*. 1987;33:297-302.
52. Glasgow LA, Liu X. Response of aggregate structure to hydrodynamic stress. *AIChE J.* 1991;37:1411-1414.
53. Curtis ASG, Hocking LM. Collision efficiency of equal spherical particles in a shear flow. *Trans Faraday Soc*. 1970;66:1381-1390.
54. Keys RO, Hogg R. Mixing problems in polymer flocculation. *Water 1978, AIChE Symposium Series*. 1978;63-72.
55. Oles V. Shear-induced aggregation and breakup of polystyrene latex particles *J of Colloid Interface Science* 1992;154:351-358.
56. Chung CB, Park SH, Han IS, Seo, IS, Yang BT. Modelling of ABS latex coagulation processes. *AIChE J*. 1998;44:1256-1265.
57. Pandya JD, Spielman LA. Floc breakage in agitated suspensions: theory and data processing strategy. *J of Colloid Interface Sci*. 1982; 90:517-531.
58. Glasgow LA, Lueche RH. Mechanisms of deaggregation for clay-polymer flocs in turbulent systems. *Ind Eng Chem Fundam*. 1980; 19:148-156.
59. Tomi D, Bagster DF. The behaviour of aggregates in stirred vessels. *Trans IChemE*. 1978;56:1-8.
60. Heath AR, Bahri PA, Fawell PD. Aggregation of calcite by polymeric flocculant, experimental observations in turbulent pipe flow. In press. AIChE J. 2005.
61. Heath AR, Fawell PD, Bahri PA, Swift JD. Estimating average particle size by focussed beam reflectance measurement (FBRM). *Particle and Particle Systems Characterisation*. 2002;19.84-95.
62. Hounslow MJ, Ryall RL, Marshall VR. A discretized population balance for nucleation, growth and aggregation. *AIChE J*. 1988;34: 1821-1832.
63. Kohler HH. Thermodynamics of Adsorption from solution. In: Dobias B. *Coagulation and Flocculation: Theory and Applications*. USA: Marcel Dekker; 1993.
64. Hughes MA. Coagulation and Flocculation. In: Svarovsky L. *Solid-Liquid Separation*.4th ed. UK: Butterworth-Heinmann; 2000.
65. Atteia O. Evolution of size distributions of natural particles during aggregation: modelling versus field results. *Colloids and Surfaces A - Physicochem and Eng Aspects*. 1998;139:171-188.
66. Gardner KH, Theis TL. A unified kinetic model for particle aggregation. *J of Colloid and Interface Sci.* 1996;180:162-173.
67. Gruy F, Saint-Raymond H. Turbulent coagulation efficiency. *J of Colloid Interface Sci*. 1997;185:281-284.
68. Kusters KA, Wijers JG, Thoenes D. Aggregation kinetics of small particles in agitated vessels. *Chem Eng Sci*. 1997;52:107-121.
69. Lawler DF. Physical aspects of flocculation: from microscale to macroscale. *Wat Sci Tech*. 1993;27:165-180.
70. Lu S, Ding Y, Guo J. Kinetics of fine particle aggregation in turbulence. *Advances in Colloid and Interface Sci*. 1998;78:197-235.
71. Wigsten AL, Stratton RA. Polymer adsorption and particle flocculation in turbulent flow. In: Goddard ED, Vincent B. *Polymer Adsorption and Dispersion Stability, ACS Symp. Ser. 240. Am Chem Soc*. 1984;429-444.
72. Wistrom A, Farrell J. Simulation and system identification of dynamic models for flocculation control. *Wat Sci Tech*. 1998;37:181-192.
73. Gregory J. Stability and flocculation of suspensions. In: Shamlou PA. *Processing of Solid-Liquid Separations.* UK: Butterworth-Heinemann; 1993;59-92.
74. Bagster DF. Aggregate behaviour in stirred vessels. In: Shamlou PA. *Processing of Solid-Liquid Separations.* UK: Butterworth-Heinemann; 1993;26-58.
75. Mühle K. Floc stability in laminar and turbulent flow. In: Dobias B. *Coagulation and Flocculation: Theory and Applications*. USA: Marcel Dekker, 1993;355-282.
76. Hogg R. Polymer adsorption and flocculation. In: Laskowski JS. *Polymers in Mineral Processing*. Symposium organized by: The Canadian Institute of Mining, Metallurgy and Petroleum. Quebec, Canada: August 1999. *Met Soc*. 1999;3-17.
77. Hogg R. The role of polymer adsorption kinetics on flocculation. *Colloids and Surfaces*. 1999;146:253-263.
78. Dahlstrom DA, Fitch EB. Thickening. In: Weiss NL. *SME Mineral Processing Handbook*. American Institute of Mining, Metallurgical, and Petroleum Engineers, Inc. USA: Kingsport Press; 1985.
79. Perry HR, Green DW. *Perry's Chemical Engineers Handbook*. 7th ed. New York: McGraw-Hill; 1997.
80. Svarovsky L. *Solid-Liquid Separation.* 4th ed. UK: Butterworth-Heinemann; 2000.
81. Nagata S. *Mixing Principles and Applications*. John Wiley; 1975.
82. Etchells AW, Short DGR. Pipeline mixing - a user's view part 1 - turbulent blending. *6th European Conference on Mixing*. Pavia: Italy; 24-26 May; 1988;539-544.
83. Godfrey JC, Amirtharajah A. Mixing in liquids. In: Amirtharajah, A. *Mixing in Coagulation and Flocculation*. USA: American Water Works Association Research Foundation; 1991;35-79.
84. Smith DKW, Kitchener JA. The strength of aggregates formed in flocculation. *Chem Eng Sci*. 1978;33:1631-1636.
85. Ray DT, Hogg R. Agglomerate breakage in polymer-flocculated suspensions. *J of Colloid Interface Sci*. 1987;116:256-268.
86. Bird RB, Stewart WE, Lightfoot EN. *Transport Phenomena*. New York: Wiley; 1960.
87. Govier GW, Aziz K. *The Flow of Complex Mixtures in Pipes.* Melbourne: Van Nostrand Reinhold Company; 1972.
88. Wasp EJ, Kenny JP, Gandhi RL. *Solid-Liquid Flow Slurry Pipeline Transportation*. Germany: Trans Tech Publications; 1977.
89. Blasius H. Das Ähnlichkeitsgesetz bei Reibungsvorgängen in Flüssigkeiten. *Forschn. Gebiete Ingenierw*. 1913;131.
90. Einstein A. Eine neue bestimmung der molekül-dimensionen. *Annalew der Physik*. 1908;19:289-306.
91. Liu S, Masliyah JH. Flow of suspensions in pipelines. In: Schramm LL. *Suspensions, Fundamentals and Applications to the Petroleum Industry*. USA: Library of Congress Cataloguing-in-publication Data; 1996.
92. Fleer GJ, Scheutjens JMHM. Modelling polymer adsorption, steric stabilization and flocculation. In: Dobias B. *Coagulation and Flocculation: Theory and Applications*. USA: Marcel Dekker, 1993;209-263.
93. Strenge K. Structure formation in disperse systems. In: Dobias B. *Coagulation and Flocculation: Theory and Applications*. New York: Marcel Dekker; 1993;265-320.
94. Schramm LL. *Suspensions, Fundamentals and Applications in the Petroleum Industry*. USA: A Chem Soc. 1996.

95. Bustos MC, Concha F, Burger R, Tory EM. *Sedimentation and Thickening*. London: Kluwer Academic Publishers; 1999.
96. Mills PDA, Goodwin JW, Grover BW. Shear field modification of strongly flocculated suspensions - aggregate morphology. *Colloid Polymer Sci*. 1991;269:949-963.
97. Jiang Q, Logan BE. Fractal dimensions of aggregates determined from steady-state size distributions. *Environ Sci Technol*. 1991;25: 2031-2038.
98. Williams RA, Simons SJR. Handling colloidal materials. In: Williams RA. *Colloid and Surface Engineering, Applications in the Process Industries*. UK: Butterworth-Heinemann; 1992.
99. Stumm W, Morgan JJ. *Aquatic Chemistry*. 3rd ed. New York: Wiley-Interscience; 1996.
100. Dyer KR, Manning AJ. Observation of the size, settling velocity and effective density of flocs, and their fractal dimensions. *J of Sea Res*. 1999;41:87-95.
101. Pearse MJ. *Gravity Thickening Theories: A Review*. UK: Warren Spring Laboratory, Dept. of Industry; 1977.
102. Sikora MD, Stratton RA. The shear stability of flocculated colloids. *Tappi* 1981;64:97-101.
103. Leu R, Ghosh MM. Polyelectrolyte characteristics and flocculation. *J of the A Water Works Ass*. 1988;80:159-167.
104. Williams RA, Peng SJ, Naylor A. In situ measurement of particle aggregation and breakage kinetics in a concentrated suspension. *Powder Technol*. 1992;73:75-83.
105. Hogg R. Flocculation and dewatering. *Int J Miner Process*. 2000;58: 223-236.
106. Heath AR, Fawell PD, Bahri PA, Swift JD. Population balance modelling of flocculation processes. *CHEMECA*. Perth; September, 1999.
107. Geffroy C, Persello J, Foissy A, Lixon P, Tournilhac F, Cabane B. Molar mass selectivity in the adsorption of polyacrylates on calcite. *Colloids and Surfaces, A: Physicochem and Eng Aspects.* 2000;162: 107-121.
108. Barnes HA, Holbrook SA. High concentration suspensions: preparation and properties. In: Shamlou PA. *Processing of Solid-Liquid Separations.* UK: Butterworth-Heinemann; 1993.
109. Healy TW. Flocculation-dispersion behavior of quartz in the presence of a polyacrylamide flocculant. *J of Colloid Sci*. 1961;16:609-617.
110. Thomas DG. Turbulent disruption of flocs in small particle size suspensions. *AIChE J*. 1964;10:517-523.
111. Kobayashi M, Adachi Y, Ooi S. Breakup of fractal flocs in a turbulent flow. *Langmuir*. 1999;15:4351-4356.

Manuscript received Jun. 13, 2005, and revision received Nov. 9, 2005.